AIAA SciTech Forum
8-12 January 2024, Orlando, FL
AIAA SCITECH 2024 Forum

10.2514/6.2024-2444

Investigation of the Aeroelastic Response of a Compliant Panel

Lior Poplingher [1], Noam Touati [2] and Daniella E. Raveh [3]
Technion-Israel Institute of Technology, Haifa, 3200003, Israel

Alex Shousterman [4] and Yuval Levy [5]
Israeli CFD Center, Caesarea Industrial Park, 3088900, Israel

The paper presents a numerical investigation of the aeroelastic response of a compliant panel exposed to a supersonic flow at Mach 2. The thin panel configuration is studied as part of the 3rd Aeroelastic Prediction Workshop (AePW-3), high-speed working group, and is representative of a metallic skin panel of high-speed vehicles. The main goal of the current study is to investigate the panel's response at different physical and numerical conditions to verify the implemented methodology against known trends and behavior of the compliant panel and to provide the building blocks for subsequent aeroelastic investigations of the compliant panel within the CFD solver with a high-fidelity flow solution for more complex cases with shock impingement. The results were compared to previous studies and were found to be consistent with previous observations.

I. Introduction

The High-Speed Working group (HSWG) of the third Aeroelastic Prediction Workshop (AePW-3) aims at assessing state-of-the-art computational capabilities for the prediction of fluid-structure interaction (FSI) at high speeds. The HSWG studies two test cases representing fundamental applications of FSI at high speeds. We focus on the *AFRL/SSC RC-19 Clamped Thin Panel* test case (which we designate as AFRL-RC-19) [1] that concerns a clamped compliant panel flushed with the ceiling of the RC-19 supersonic wind tunnel of the Air Force Research Laboratory (AFRL) at Mach 2 with a pressurized cavity located on the opposite side of the panel. This test case is representative of metallic skin panels of reusable high-speed vehicles. The experimental study of this configuration examined different flow configurations, including shock impingement on the panel.

Panel flutter was investigated in numerous studies over the years [2, 3]. The panel behavior with dynamic pressure can be divided into pre-flutter and post-flutter responses. For dynamic pressures lower than the flutter boundary, the panel mainly responds to turbulent pressure fluctuations in the boundary layer, while the post-flutter response is characterized by almost harmonic oscillations with increasing amplitude [2]. At these conditions, the panel's response can reach amplitudes with a magnitude of several panel thicknesses. It is noteworthy that Brouwer et al. [4] also indicated that the pressure fluctuations in the turbulent boundary layer, which are not accounted for in most analytical studies, play a significant role in post-flutter conditions and may affect the prediction of the aeroelastic response compared to experiments.

The flutter response of a compliant panel depends on several factors that mainly affect the stiffness of the panel. These factors include 1) Static pressure difference, 2) Thermal stresses and buckling, 3) In-plane stiffness, and 4) Cavity acoustics. The static pressure difference acting on the panel due to the pressure modulation in the cavity results in a pre-stress on the panel which stiffens it, increases the flutter boundary dynamic pressure, and, at post-flutter conditions, reduces the aeroelastic response amplitude. Thermal stresses are imposed on the panel by heating it or merely by the difference between the heating rates of the thin panel and its support. Overall, heating the panel induces compressive stresses and reduces the panel stiffness. More importantly, sufficiently large thermal stresses might cause thermal buckling of the panel. The response of a buckled panel depicts unique characteristics that are no longer simply harmonic or periodic. The buckling of the panel may result in co-existing equilibrium states that the panel crosses throughout the response. Brouwer et al. [4] obtained two different trends with increasing temperature differences on the panel. For near-zero static pressure difference, increasing the temperature difference results in increased response amplitude, while

[1]Graduate Student, Faculty of Aerospace Engineering, lior.pop@campus.technion.ac.il.
[2]Undergraduate Student, Faculty of Aerospace Engineering, noamtouati@campus.technion.ac.il.
[3]Professor, Faculty of Aerospace Engineering, AIAA Associate Fellow, daniella@technion.ac.il.
[4]Software Specialist, alex@iscfdc.com.
[5]CEO, yuval@iscfdc.com.

for non-zero static pressure difference, the opposite occurs. Although these behaviors seem contradictory, they appear to be the result of fundamentally different physical responses which are still not fully understood.

The effect of in-plane boundary stiffness and cavity acoustics was investigated by Dowell and collaborators [5, 6]. Piccolo Serafim et al. [6] showed that the effect of cavity acoustics on the natural frequencies of the panel is minor and its effect can be neglected when considering the aeroelastic response. The in-plane boundary conditions effect is pronounced and appears to require fine-tuning to match the experimental setup. Further information is provided in Sec. III.A.

The main goal of the current study is to investigate the aeroelastic response of the panel for the test case without shock impingement, using a low-order aerodynamic model based on Piston theory and a non-linear structural model based on the work of Freydin and Dowell [5]. This is pursued to verify the implemented methodology against known trends and behavior of the compliant panel aeroelastic response and to provide the building blocks for subsequent aeroelastic investigations of the compliant panel within the CFD solver with a high-fidelity flow solution for more complex cases with shock impingement.

II. Test Case

The AFRL-RC-19 test case includes a compliant panel embedded within the ceiling of Research Cell 19 (RC-19), which is a continuous supersonic wind tunnel operated by the Air Force Research Laboratory (AFRL). The panel is exposed to a supersonic flow at a nominal Mach number of 2. The experimental setup and results are described by Brouwer et al. [1]. Herein, we only provide some details of the experimental setup and test conditions. Figure 1 shows a schematic of the test section with the panel dimensions provided in Table 1. Both rigid and flexible panels were tested. A variable-angle shock generator was placed at the bottom of the test section and a pressurized cavity was located on the opposite side of the panel. During experiments, the cavity pressure was modulated (and measured using a Kulite inside the cavity) in order to excite a dynamic response of the panel. In addition, the temperature difference between the panel and its surrounding support was measured using two type-K thermocouples placed on the inner part of the panel and the thick frame surrounding it. Additional measured data include full-field digital image correlation (DIC) measurements that provide the entire panel deflections over time, Laser Doppler Vibrometer (LDV) used to record panel velocities at a fixed point, pressure data from Kulites positioned upstream and downstream of the panel, high-speed Schlieren imaging, and pressure-sensitive paint (PSP) data. In the tests, the shock generator was positioned in 4 different angles of 0° (i.e., no shock generator), 4°, 8°, and 12°.

Two sets of flow conditions are available from the experimental data: The *measured experimental* conditions, as reported in the experimental study by Brouwer et al. (provided in communications of the AePW-3), and the *nominal* flow conditions, defined for all different shock-generator configurations, provided by Brouwer et al. [1]. The flow conditions are defined in Table 2. The focus of the current study is on the measured experimental conditions without shock impingement.

Table 1 Panel dimensions for the AFRL-RC-19 test case

Parameter	Value
Panel length, a [m]	0.254
Panel width, b [m]	0.127
Panel thickness, h [m]	6.35×10^{-4}

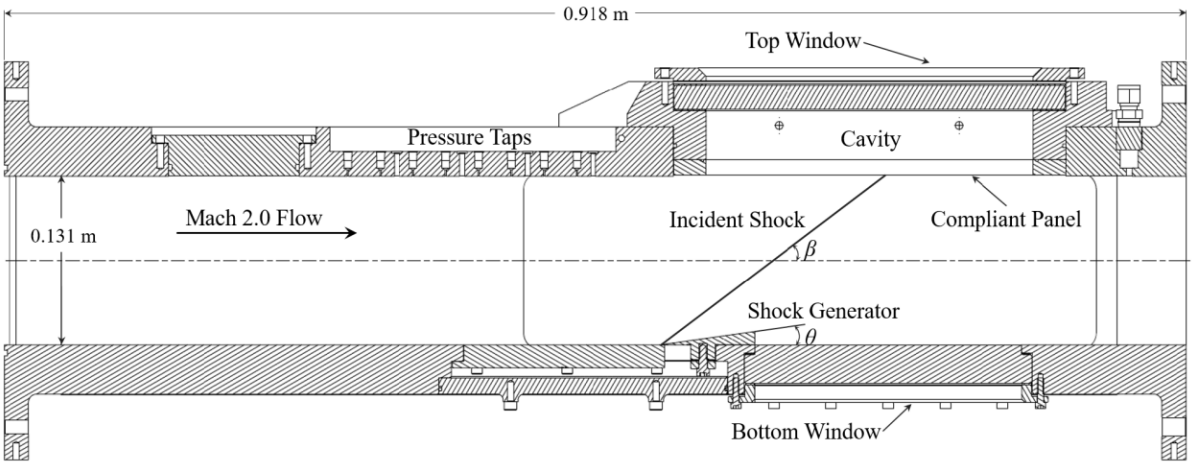

Fig. 1 Test section showing the pressure taps, shock generator, thin panel, and cavity for the AFRL-RC-19 test case (taken from AePW-3 website)

Table 2 Flow conditions for the AFRL-RC-19 test case

Designation	Mach number	Pressure [Pa]	Temperature [K]
Nominal [1] ($\theta = 0°, 4°, 12°$)	2	44093	216.1
Experiment ($\theta = 0°$)	1.94	48753	221.5
Experiment ($\theta = 4°$)	1.94	48548	220.18
Experiment ($\theta = 12°$)	1.94	48377	220.13

III. Computational Setup

The compliant panel experiences deflections in the order of 2-3 panel thicknesses. This deflection introduces a non-linear structural response in the form of added stiffness, which varies non-linearly with the deflection. To simulate the aeroelastic response of the panel, a non-linear structural model based on the work by Freydin and Dowell [5] was implemented using aerodynamic modeling based on Piston theory. The complete formulation of the model can be found in Ref. [5]. Herein, we provide only a short description of the model.

A compliant panel with length a, width b, and thickness h is considered. Although the panel is fully clamped concerning its transverse displacement (w), finite stiffness (β_{BC}) is allowed for the in-plane displacements (u and v). The coordinate system for the panel is illustrated in Fig. 2. The x-axis is in the streamwise direction, while the y-axis is in the crosswise direction. The origin is located at the middle of the upstream edge of the panel, such that the panel extents are $0 < x < a$ and $-b/2 < y < b/2$. Note that according to this definition, a positive transverse displacement indicates deflection *toward the flow*.

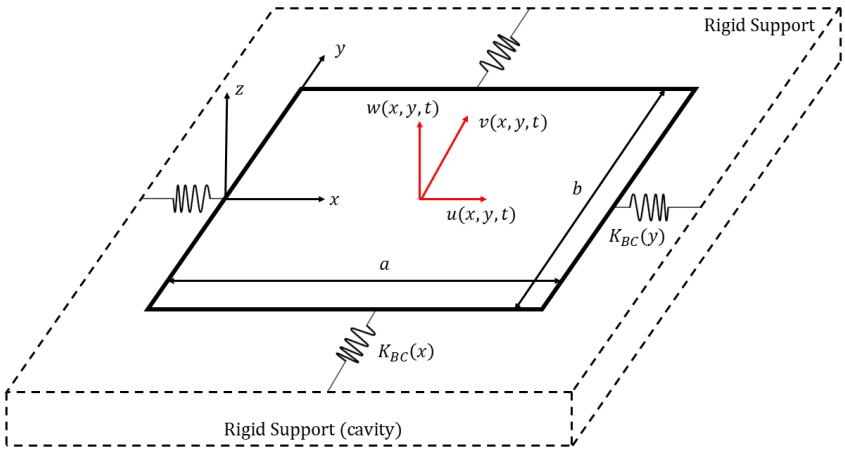

Fig. 2 Coordinate system for the compliant panel

In the aeroelastic analysis, we solve for the panel's transverse displacement as a function of time. The physical displacements are represented as a sum of assumed modes, which are the clamped panel's mode shapes. These are used to formulate the equations of motion for the transverse and in-plane displacements via Lagrange's equations [5]. The expansion of the structural displacements is given by

$$w = \sum_{i}^{N_w} w_i(t)\psi_i^w(x,y) \tag{1}$$

$$u = u_R(t)\psi_R^u(x,y) + \sum_{i}^{N_u} u_i(t)\psi_i^u(x,y) \tag{2}$$

$$v = v_R(t)\psi_R^v(x,y) + \sum_{i}^{N_v} v_i(t)\psi_i^v(x,y) \tag{3}$$

The terms noted with subscript R correspond to a rigid-body rotation mode that generates displacements in both u and v (a rigid translation mode is included inherently in the summation for $i = 0$). Note that $u_R(t) = v_R(t)$ as both describe rigid body rotation. The mode shapes, $\psi_i^w(x,y)$, for the transverse displacement are chosen such that they satisfy all-clamped boundary conditions at all panel edges. The mode shapes for the in-plane displacements, $\psi_i^{u/v}(x,y)$, are chosen to satisfy all-free boundary conditions to allow the inclusion of finite in-plane stiffness. N_u, N_v, and N_w are the total number of modes used in the analysis. The modal displacements are w_i, u_i, and v_i, determining the contribution of each mode shape to the physical displacement.

The shapes used are based on the analytical modes of the one-dimensional panel in the x (length) and y (width) directions. Figure 3 shows sample modes of the transverse displacement, where the modes are sorted by their natural frequency. The mode shapes are similar to the experimentally identified mode shapes (Fig. 4 in Ref. [1]). It is evident that the all-clamped boundary conditions are satisfied.

A key parameter of the structural model formulation is the generalized force, that is, the force acting on the panel in modal coordinates. The generalized force represents the effect of the pressure exerted on the panel by the incoming flow and a possible static pressure difference acting on the panel due to the difference between the cavity pressure (which is modulated in the experiments) and the pressure due to the flow.

In the context of the current modeling, the aerodynamic pressure variation on the panel due to the panel's displacement and velocity in the transverse direction is computed based on 1st order linear Piston Theory (PT):

$$\Delta p_{PT} = p(x,y,t) - p_\infty = \gamma p_\infty \left(\frac{v_n}{a_\infty}\right) = \frac{\rho_\infty U_\infty}{M_\infty}\left(\frac{\partial w}{\partial t} + U_\infty \frac{\partial w}{\partial x}\right) \tag{4}$$

Note that the reference pressure of classical PT is the freestream pressure, p_∞, such that the pressure difference provided by PT is (per Ref. [5] notation) - $\Delta p_{PT} = p(x,y,t) - p_\infty$. A different variant of PT, known as Enriched PT,

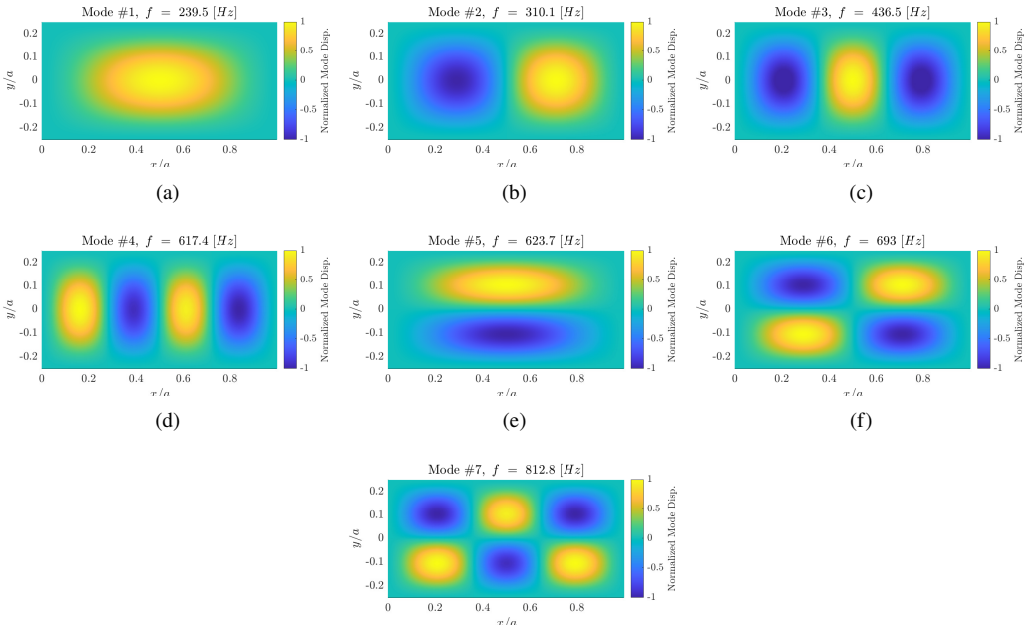

Fig. 3 Sample panel modal shapes for the transverse displacement

can be used to include the effects of boundary layers and shock impingement in a similar formulation. See Ref. [7] for details. The PT pressure difference is then used to compute the generalized forces in the modal coordinates n, Q_n^{PT}, by projecting the pressure difference on the modal basis of the transverse displacement.

Another contribution to the forces acting on the panel (and consequently the generalized force) that is accounted for is the static pressure difference acting on the panel that is *independent* of the panel motion (i.e., independent of time). This contribution stems from the pressure difference between the free surface of the panel (which is exposed to the flow) and the internal pressure in the cavity (p_c). The static pressure difference can be distributed or constant along the panel. In general

$$\Delta p_s(x, y) = p_s(x, y) - p_c \tag{5}$$

It is important to note that given the general definition of the pressure difference on the panel and the coordinate system defined in Fig. 2, the sign convention is:

1) Positive transverse displacement ($w > 0$) corresponds to displacement toward the flow with $\Delta p_s < 0$
2) Negative transverse displacement ($w < 0$) corresponds to displacement toward the cavity with $\Delta p_s > 0$

A. In-plane Stiffness

The in-plane stiffness parameter, β_{BC}, is defined in Eq. 6

$$\beta_{BC} = \frac{K_{BC} a}{E h} \tag{6}$$

where K_{BC} is the in-plane stiffness (in [Pa]), represented by the springs in Fig. 2, that can be measured experimentally through a vibration test.

As β_{BC} increases, the panel is stiffer in the in-plane direction. That is, when $\beta_{BC} \to \infty$, the panel is fully clamped with zero in-plane deformation at the boundary, while for $\beta_{BC} \to 0$, the panel is free to move in the in-plane directions at the boundaries. Freydin and Dowell [5] used the in-plane stiffness as a calibration parameter to match analytical results with experimental data. Piccolo Serafim et al. [6] studied the effect of β_{BC} on the RC-19 panel natural frequencies and response compared to experimental data and obtained significant responses for $\beta_{BC} \approx 4$. The responses nature (i.e., periodic or "chaotic", as termed in Ref. [1]) varied for different β_{BC} values.

Since the panel was manufactured from a single block of steel, it is expected that there will be very little in-plane deflections at the panel's boundaries. Thus, we focus our study on $\beta_{BC} = 100$. Although this value is significantly higher than the values reported in Ref. [6] to yield panel oscillations, and different values of β_{BC} will produce different results, we chose to use $\beta_{BC} = 100$ since it captures the close-to-fully-clamped conditions in the test.

B. Stiffness Calibration

In the experimental work of Brouwer et al. [1], the natural mode shapes of the panel (Fig. 3) and their corresponding natural frequencies and damping values were measured before the installation of the panel in the wind tunnel. This data can be used to calibrate the linear stiffness matrix [5].

The updated natural frequencies are used for the first seven modes and provided in Tab. 3. Note that the FE-based natural frequencies were obtained from the solution of the original (un-calibrated) eigenproblem of the panel and the updated frequencies are based on information from Refs. [1, 4].

Table 3 Calibrated and un-calibrated natural frequencies (in Hz) of the compliant panel

Source	f_1	f_2	f_3	f_4	f_5	f_6	f_7
FE-based	239.5	310.1	436.5	617.4	623.7	693	812.8
Measured	260	302	418	593	618	679	771

The same calibration procedure can be applied to the structural damping matrix by updating specific values of ζ_n to those modes that were measured experimentally. In the current study, we focus on the effect of the stiffness calibration alone and assume zero structural damping for all modes.

IV. Results

A. $\Delta T - \Delta P$ Maps

As noted in Sec. I, two of the main parameters that affect the aeroelastic response of the panel are the static pressure differential acting on it due to the cavity pressure modulation (ΔP) and the temperature difference between the panel and its support (ΔT). The cavity pressure is known with high accuracy since it is measured directly in the cavity with a Kulite. In contrast, the panel temperature was only measured at a single point, and therefore the ΔT value provided from the test data has significantly greater uncertainty. It is therefore beneficial to explore the effect of these two parameters in a range of values (rather than focusing on the values provided from the test) on the aeroelastic response of the panel. This is shown in Fig. 4 for both the calibrated and un-calibrated setups (Sec. III.B) and using an in-plane stiffness parameter of $\beta_{BC} = 100$. The overall behavior of the results agrees well with the numerical prediction of Brouwer et al. [4]. The most prominent response is obtained around $\Delta P = 0$, which is consistent with the contribution of the pressure difference to the stiffening of the panel. For $\Delta P = 0$, as ΔT increases, the response amplitude also increases. Above $\Delta T = 5$ K, the panel is assumed thermally buckled [4]. For a thermally buckled panel, it was shown that complex aeroelastic responses can occur as the panel crosses between different equilibrium states. The oscillations' amplitude increases with ΔT, corresponding to the increased deformation of the equilibrium states.

Comparing the calibrated vs. un-calibrated responses, the regions of panel oscillations for the un-calibrated map are more sparse and with overall lower oscillation amplitude. This is still not fully understood and requires a point-to-point inspection to further investigate the effect of slight changes in the natural frequencies of the panel. It is noteworthy that Piccolo Serafim et al. [6] showed the effect of considering different stiffness constructions (that is, with coupled-cavity acoustics, with aerodynamics added stiffness, etc.). It was shown that the first mode frequency generally decreases with added stiffness elements, although other modes might depict different trends. It was also observed that increasing the in-plane stiffness parameter, β_{BC}, increases significantly the natural frequencies of the panel. Thus, a rigorous analysis of the natural modes due to different stiffness elements is required, considering further decomposition of the different elements, e.g., separating the contribution of ΔP and ΔT.

Figures 5 and 6 show the modal contributions corresponding to the same conditions presented in Fig. 4. It can be

observed that the first mode contribution is the most dominant across the $\Delta T - \Delta P$ maps (calibrated and un-calibrated). There are some regions in the un-calibrated $\Delta T - \Delta P$ map in which the second mode is more dominant, however, these regions are of small overall amplitude, and they significantly reduce when considering the calibrated setup.

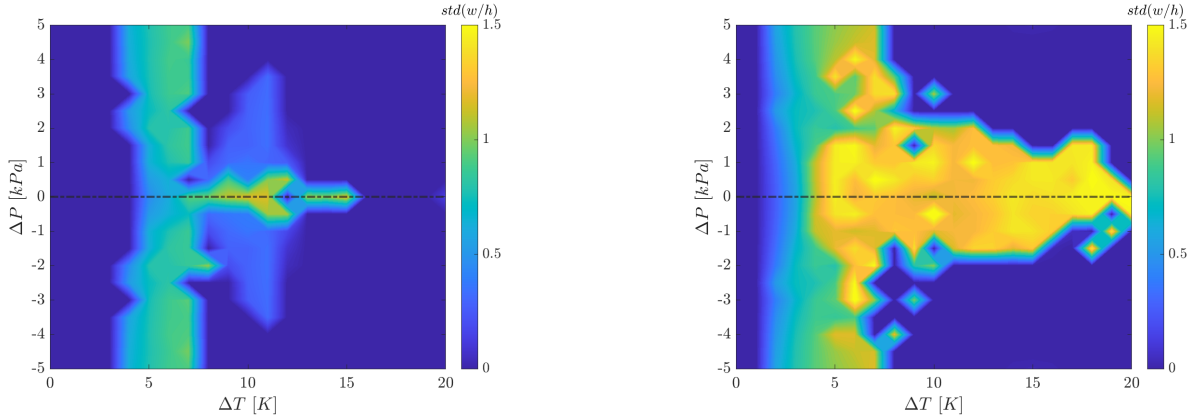

(a) Un-calibrated (b) Calibrated

Fig. 4 $\Delta T - \Delta P$ **maps of standard deviation of the panel oscillations at mid-panel and** $x/a = 0.75$ **for in-plane stiffness of** $\beta_{BC} = 100$

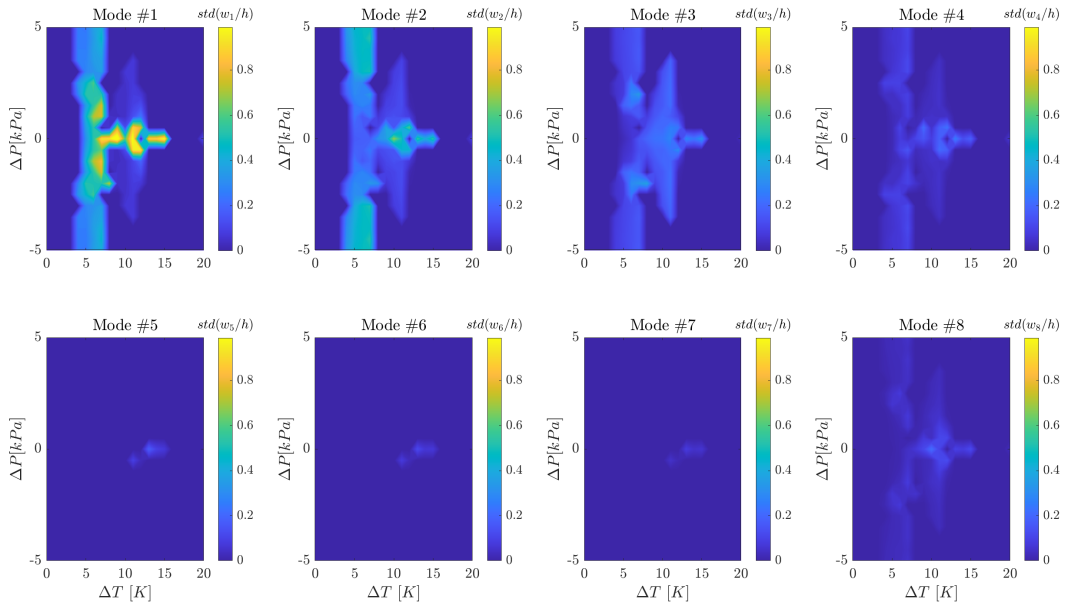

Fig. 5 $\Delta T - \Delta P$ **maps of modal contributions for un-calibrated setup and in-plane stiffness of** $\beta_{BC} = 100$

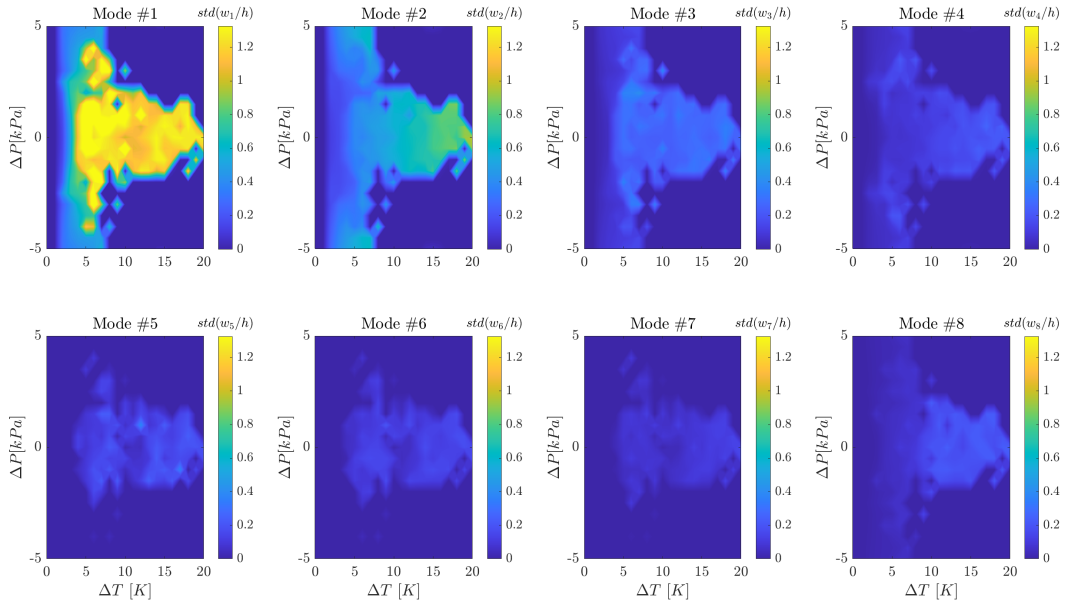

Fig. 6 $\Delta T - \Delta P$ maps of modal contributions for calibrated setup and in-plane stiffness of $\beta_{BC} = 100$

B. Effect of Static Pressure Difference Distributions

The shock-impingement cases pose difficulties in the prediction of the pressure difference on the panel both static (due to cavity pressure modulation) and dynamic (due to the panel movement). It is clear that when these cases are considered a more complex treatment of the pressure difference will be required to account for the shock impingement effect. As a first step towards this treatment, we examine the effect of using different representations of the static pressure difference on the aeroelastic response of the panel.

Figure 8 shows the mean and standard deviation of the panel displacement at mid-panel and $x/a = 0.75$ for in-plane stiffness of $\beta_{BC} = 100$, vs. the temperature difference, using several options for the static pressure difference: 1) Based on the time-averaged static pressure distribution measurements (provided in the AePW3), 2) Based on a RANS CFD steady-state pressure distribution, and 3) Constant distribution based on the mean of the two distributions above (noted in the legend). The first two pressure difference distributions are shown in Fig. 7. The experimental data was obtained by mapping the time-averaged static pressure measurements onto the CFD mesh. It can be seen that the distributions are quite different. The CFD-based distribution shows very little span-wise and chord-wise variation. The constant span-wise distribution is due to the symmetry boundary conditions applied for the wind-tunnel side walls, while the chord-wise distribution is also minimal due to the benign flow conditions and wind-tunnel geometry. In contrast, the experimentally measured distribution shows irregular behavior (probably due to the sparse pressure sensors).

Considering the use of mean pressure differences, the behavior of the responses is similar for both the CFD-based and experimental averages. The differences between the two responses are due to the different mean values, as observed in Fig. 4, where lower pressure difference results in a larger range of temperature difference values with panel oscillations. The use of pressure distributions shows distinct results comparing both the CFD and experiment data and also the mean vs. distributed static pressure difference. It can be observed that using the CFD-based distributed pressure difference, the aeroelastic response at low ΔT diminishes, while the responses at higher ΔT are similar to the mean-based pressure difference. For the experimental distribution, the results are similar using the mean and distributed data, except for several data points that are shifted to lower ΔT values.

The results using different pressure difference setups do not indicate a clear trend. However, they illustrate the sensitivity of the responses to the chosen methodology of applying a static pressure difference, and more fundamentally, to the static loading on the panel. This should be carefully considered for the more complex cases including shock impingement.

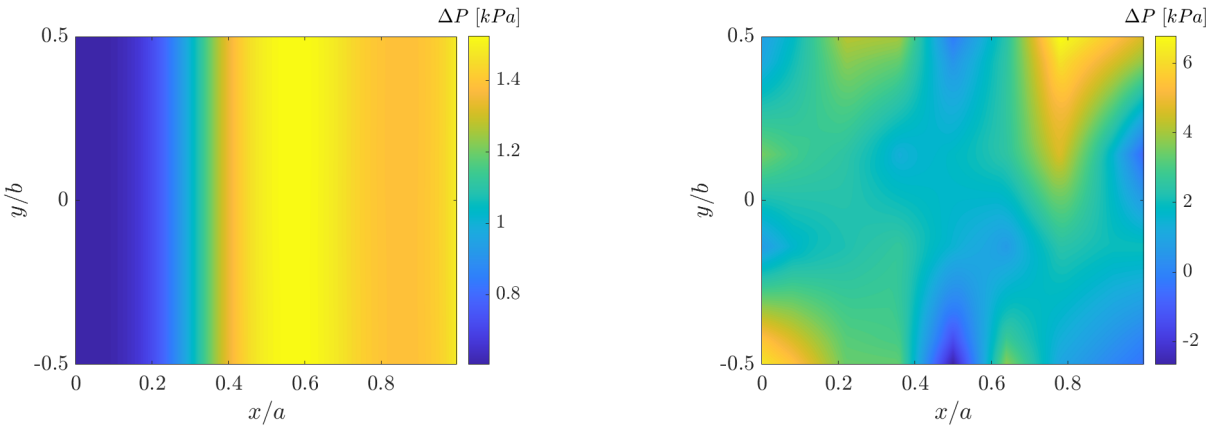

(a) CFD (b) Experiment

Fig. 7 Pressure difference distributions obtained using steady-state RANS CFD solution and experimental time-averaged pressure taps measurements with p_c = 50.4 kPa

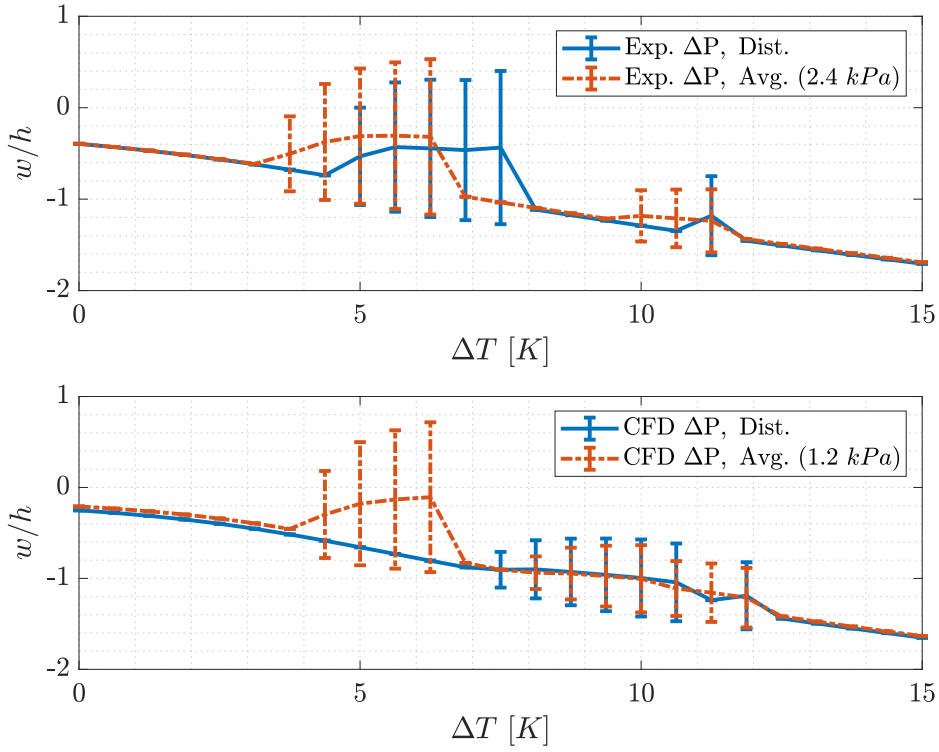

Fig. 8 Effect of different pressure difference setups on the aeroelastic response of the panel for different temperature differences and in-plane stiffness of β_{BC} = 100

C. Analysis of Specific Data Points

In this section, we investigate the aeroelastic responses at specific data points to highlight some physical aspects of the responses. Figure 9 shows the responses at mid-panel and x/a = 0.75, their frequency content, and modal contributions. These were computed for different temperature differences using the calibrated setup, β_{BC} = 100, and

the experimental static pressure difference distribution.

It can be observed that as ΔT increases, the amplitude of the response also increases from $1.5h$ for $\Delta T = 2.5$ K to $5.2h$ for $\Delta T = 10$ K. This amplitude increase corresponds to ΔT exceeding the buckling temperature of the panel (reported at 5.6 K in Ref. [4]).

The response for $\Delta T = 2.5$ K (below the buckling temperature) is periodic with a distinct frequency peak near the first mode of the panel, which is also the most dominant in the modal participation. The response for $\Delta T = 5$ K is characterized by two distinct peaks in the frequency content near the first and third modes. This is consistent with the dominant participation of these modes. In contrast, for the higher ΔT, the response becomes irregular and consists of broadband amplification at frequencies between the first and third modes, and concentrated at a frequency near the second mode. The modal participation, compared to the lower ΔT cases, is characterized by a dominant first mode, while higher modes show decreasing participation. This behavior is consistent with the observations of Brouwer et al. [4].

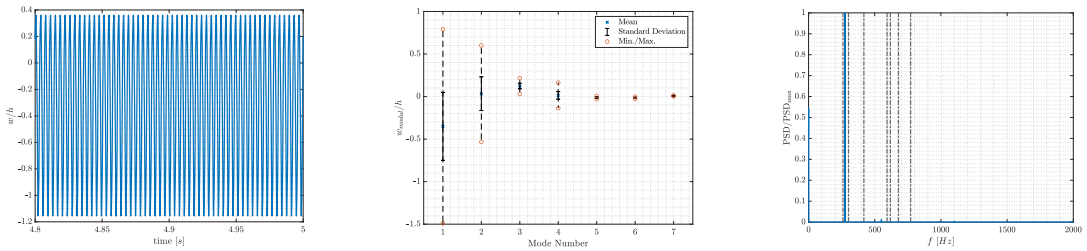

(a) $\Delta T = 2.5$ K

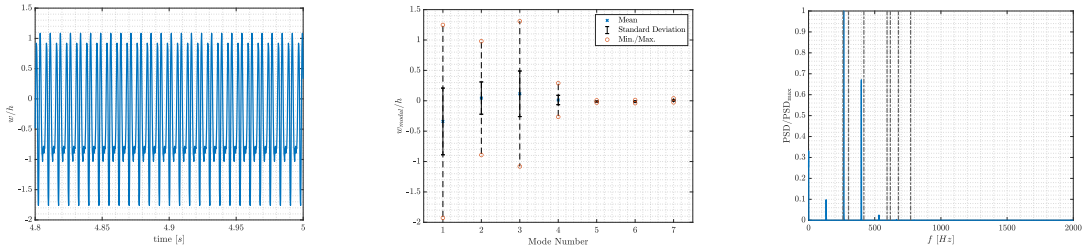

(b) $\Delta T = 5$ K

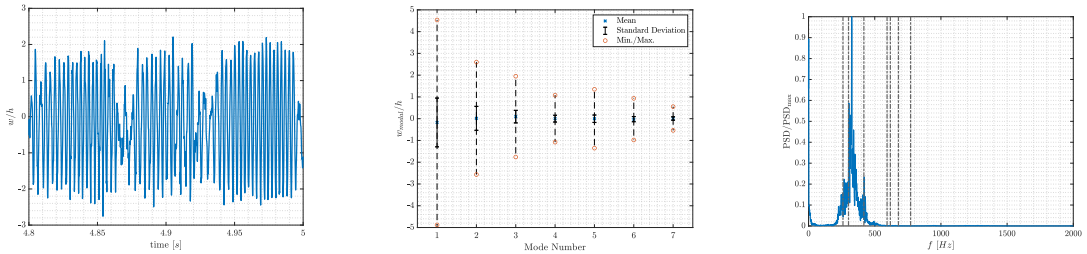

(c) $\Delta T = 10$ K

Fig. 9 Characteristics of the aeroelastic response of the panel for $\beta_{BC} = 100$ and different temperature differences

V. Summary and Conclusions

The current study presents the use of a non-linear structural model coupled with a low-order aerodynamics model based on Piston theory to predict the aeroelastic response of a compliant panel that was experimentally investigated in the RC-19 wind tunnel as part of the AePW3.

The main goal of the current study was to investigate the panel's response at different physical and numerical conditions to verify the implemented methodology against known trends and behavior of the compliant panel aeroelastic response and to provide the building blocks for subsequent aeroelastic investigations of the compliant panel within the CFD solver with a high-fidelity flow solution for more complex cases with shock impingement. The results were compared to previous studies and were found to be consistent with previous observations.

It is noteworthy that all the presented results were obtained using a high in-plane stiffness parameter ($\beta_{BC} = 100$). We assume that this higher value, which was not fully considered in previous studies employing the same structural model, captures the close-to-fully-clamped conditions in the test. While this parameter was used in previous studies to calibrate numerical results against experimental data, using a more physically adequate (to the specific experimental setup) value results in panel responses consistent with both experimental and numerical observations.

The effect of stiffness calibration was studied using maps of panel response amplitude for different combinations of static pressure difference and temperature difference. It was found that using stiffness calibration (via the update of the eigenvalues of the linear stiffness matrix), the responses are of higher amplitude and at an extended range of ΔP and ΔT combinations.

Different setups for the static pressure difference, i.e., distributed vs. constant and using CFD solution vs. experimental data, were also examined. It was found that the responses are similar except for some specific values of temperature difference.

Finally, the responses at specific data points were presented, depicting similar trends observed in previous studies. Mainly, the effect of thermal buckling was observed to increase the response's amplitude and change it to a more irregular response as the temperature difference was increased.

References

[1] Brouwer, K. R., Perez, R. A., Beberniss, T. J., Spottswood, S. M., and Ehrhardt, D. A., "Experiments on a Thin Panel Excited by Turbulent Flow and Shock/Boundary-Layer Interactions," *AIAA journal*, Vol. 59, No. 7, 2021, pp. 2737–2752.

[2] Dowell, E. H., "Panel flutter - A review of the aeroelastic stability of plates and shells," *AIAA Journal*, Vol. 8, No. 3, 1970, pp. 385–399. https://doi.org/10.2514/3.5680.

[3] Mei, C., Abdel-Motagaly, K., and Chen, R., "Review of Nonlinear Panel Flutter at Supersonic and Hypersonic Speeds," *Applied Mechanics Reviews*, Vol. 52, No. 10, 1999, pp. 321–332. https://doi.org/10.1115/1.3098919.

[4] Brouwer, K., Perez, R., Beberniss, T., Spottswood, S., Ehrhardt, D., and Wiebe, R., "Investigation of Aeroelastic Instabilities for a Thin Panel in Turbulent Flow," *Nonlinear Dynamics*, Vol. 104, No. 4, 2021, pp. 3323–3346. https://doi.org/10.1007/s11071-021-06571-4.

[5] Freydin, M., and Dowell, E. H., "Nonlinear Theoretical Aeroelastic Model of a Plate: Free to Fixed In-Plane Boundaries," *AIAA Journal*, Vol. 59, No. 2, 2021, pp. 658–672. https://doi.org/10.2514/1.J059551.

[6] Piccolo Serafim, L., Freydin, M., and Dowell, E. H., "Correlation of supersonic wind tunnel measurements with a nonlinear aeroelastic theoretical/computational model of a thin plate," *Journal of Fluids and Structures*, Vol. 122, 2023, p. 103981. https://doi.org/https://doi.org/10.1016/j.jfluidstructs.2023.103981.

[7] Brouwer, K. R., and McNamara, J. J., "Enriched Piston Theory for Expedient Aeroelastic Loads Prediction in the Presence of Shock Impingements," *AIAA Journal*, Vol. 57, No. 3, 2019, pp. 1288–1302. https://doi.org/10.2514/1.J057595.